Journal of Optics

PAPER • OPEN ACCESS

Dual-band electro-optically steerable antenna

To cite this article: Dmytro Vovchuk *et al* 2023 *J. Opt.* **25** 105601

View the article online for updates and enhancements.

You may also like

- Quantum steering in magnetic Heisenberg models at finite temperature
Liang Chen and Ye-Qi Zhang
- Ovipositor-inspired steerable needle: design and preliminary experimental evaluation
M Scali, T P Pusch, P Breedveld et al.
- X-ray to MR: the progress of flexible instruments for endovascular navigation
Mohamed E M K Abdelaziz, Libaihe Tian, Mohamad Hamady et al.

This content was downloaded from IP address 132.66.51.133 on 29/08/2023 at 18:30

OPEN ACCESS
IOP Publishing
Journal of Optics
J. Opt. **25** (2023) 105601 (8pp)
https://doi.org/10.1088/2040-8986/acf1ae

Dual-band electro-optically steerable antenna

Dmytro Vovchuk[1,2,4,*], Anna Mikhailovskaya[1,4], Dmitry Dobrykh[1], Toms Salgals[3] and Pavel Ginzburg[1]

[1] School of Electrical Engineering, Tel Aviv University, Ramat Aviv, Tel Aviv 69978, Israel
[2] Department of Radio Engineering and Information Security, Yuriy Fedkovych Chernivtsi National University, Chernivtsi 58012, Ukraine
[3] Institute of Telecommunications, Riga Technical University, 12 Azenes Street, Riga 1048, Latvia

E-mail: dimavovchuk@gmail.com

Received 30 April 2023, revised 7 August 2023
Accepted for publication 18 August 2023
Published 29 August 2023

Abstract

The ability to obtain dynamic control over an antenna radiation pattern is one of the main functions, desired in a vast range of applications, including wireless communications, radars, and many others. Widely used approaches include mechanical scanning with antenna apertures and phase switching in arrays. Both of those realizations have severe limitations, related to scanning speeds and implementation costs. Here we demonstrate a solution, where the antenna pattern is switched with optical signals. The system encompasses an active element, surrounded by a set of cylindrically arranged passive dipolar directors, functionalized with tunable impedances. The control circuit is realized as a bipolar transistor, driven by a photodiode. Light illumination in this case serves as a trigger, capable of either closing or opening the transistor, switching the impedance between two values. Following this approach, a compact half-a-wavelength footprint antenna, capable of switching between 6 dBi directional patterns within a few milliseconds' latency was demonstrated. The developed light activation approach allows constructing devices with multiple almost non-interacting degrees of freedom, as a branched feeding network is not required. The capability of flexible switching between multiple electromagnetic degrees of freedom opens pathways to new wireless applications, where fast beam steering and beamforming performances are required.

Keywords: steerable antenna, bipolar transistor switches, bundle conductors, optoelectronic devices, antenna radiation patterns

(Some figures may appear in colour only in the online journal)

[4] Equal contribution.
[*] Author to whom any correspondence should be addressed.

Original content from this work may be used under the terms of the Creative Commons Attribution 4.0 licence. Any further distribution of this work must maintain attribution to the author(s) and the title of the work, journal citation and DOI.

 © 2023 The Author(s). Published by IOP Publishing Ltd

1. Introduction

The ability to control the radiation pattern with high accuracy allows for establishing efficient point-to-point communication, where one or more participants can change their locations during the process. A radar, tracking a moving target in both azimuth and elevation, is one notable example. Recently, the automotive industry raised a demand for high-resolution short-range radar-based imaging systems, where high-quality fast scanning small aperture antennas are essential components [1–3]. While LIDARs can be considered a competitive technology [4, 5], they have a range of disadvantages (e.g. susceptible to weather conditions), and thus cannot serve as an ultimate replacement. Another realm is 5G communications, where beamforming with millisecond-scale latency is the enabling technology to support fast-speed broadband wireless communication [6, 7]. In all the beforehand mentioned applications, antenna devices are subject to engineering tradeoffs where high scanning speed and low cost are contradictory requirements. There are several traditional approaches to beam steering [8]. The first one is a mechanical scan, where a motor controls the angular position of a highly directive antenna. This technique is frequently used for implementing marine and airport tracking radars, where scanning speeds are not the main factor to consider [9, 10]. Another approach to beam steering is based on antenna-phased arrays. Here multiple elements are phased-locked and radiate simultaneously. While this architecture allows achieving fast all-electronic scanning, the realization of high-quality and directive beams requires employing tens or even hundreds of phase-shifting elements. This approach is used e.g. in airborne applications, where the speed and scan quality requirements predominate over-involved costs of realizations [11]. Recently, several approaches, complementary to traditional phased arrays have been proposed and demonstrated. The ability to tailor and control the laws of refraction with the help of artificially structured media (metamaterials [12–15]) opened a range of new capabilities in beam shaping and control. Carefully designed surfaces (metasurfaces) can provide capabilities to tailor properties of transmitted and reflected waves [12, 16–20]. While many metasurface studies concentrate on static configurations (e.g. [21–23]), introducing fast real-time tunability is the demanded feature. Several realizations of dynamically reconfigurable metasurfaces and metasurface-based antennas have been demonstrated (e.g. [17, 24–28]). The key underlining concept is typically based on controlling individual resonant elements within an array with electronics. For example, tunable capacitance allows shifting resonant responses of individual elements, and as a result, either amplitude or phase switchable screens are achieved [17, 29, 30] (in those realizations, obtaining scanning rates above KHz is barely possible. Also, those numbers are rarely discussed). While this type of realization does not rely on expensive phase shifters, it still requires using numerous (yet simple and cheap) electronic elements, and, even more critically, a branched set of wires to drive them. While reflect array configurations allow hiding wires behind a ground plane [31, 32], electric circuitry can significantly affect electromagnetic performances in other realizations. For example, a mesh of thin wires with subwavelength spacing will have a predominating undesired electromagnetic response. A probable solution to this problem has been demonstrated in the case of volumetric metamaterial-based scatterers [33]. It relies on driving individual meta-atoms with light. Light and light guiding materials do not interact with cm and mm waves, which enables the uncoupling of these two phenomena in the design. The interaction happens directly within an individual antenna element, where optical energy is rectified within a photoelement to drive electronics. Here we develop the concept of electro-optically driven beamforming, which allows fast manipulation over radiation patterns by arranging arrays of auxiliary optically switchable reflectors and directors around a radiating element. The optical link allows for obtaining both high switching speeds and modularity, i.e., almost any radiating element can be granted with scanning capabilities, as the constraints related to a wired feeding network are relaxed.

The manuscript is organized as follows—a single optically switchable dipolar element is introduced first and then it is integrated into an antenna device. The antenna characteristics are assessed with an emphasis on beam steering properties. The capability to grant steering capabilities for several commercial and custom-made antennas with optically switchable elements is discussed before the conclusion. A patent, encompassing the basic concept of this report was filed by us in 2020 [34].

2. Electro-optically driven element

Quite a few designs of directive antennas are based on interference phenomena between several elements [35, 36]. A representative example here is the Yagi-Uda antenna, where a set of passive elements—reflectors and directors, are responsible for a narrow beam formation. Each of them introduces a different phase lag, which is tuned by controlling the lengths of elements within the architecture. While the physical size of a resonant element cannot be controlled dynamically on a reasonably fast timescale, electric length can be governed by introducing a tunable lumped element. As the first step, we will demonstrate a design of a wirelessly tunable single element, which will be subsequently integrated within a beam steering array. Two states—'on' and 'off' correspond to either presence or absence of the illumination. Our basic component is a half-wavelength element ($\lambda/2$), formed by a pair of $\lambda/4$-length wires with a gap in between (figure 1(a)). The driving circuit consists of two photodiodes (BPW34) and a bipolar transistor (BFU730F115 NPN-type BJT) as in figure 1(b). Two photoelements are used to elevate the voltage drop to open the transistor. If the illumination power on the circuit is insufficient, the element acts as a cut. After passing a threshold, the diode becomes a short circuit.

Figure 1(c) demonstrates the forward scattering spectra of the system at its two states. Wire dimensions are length $l = 72$ mm and radius $r = 0.5$ mm. The gap in the middle

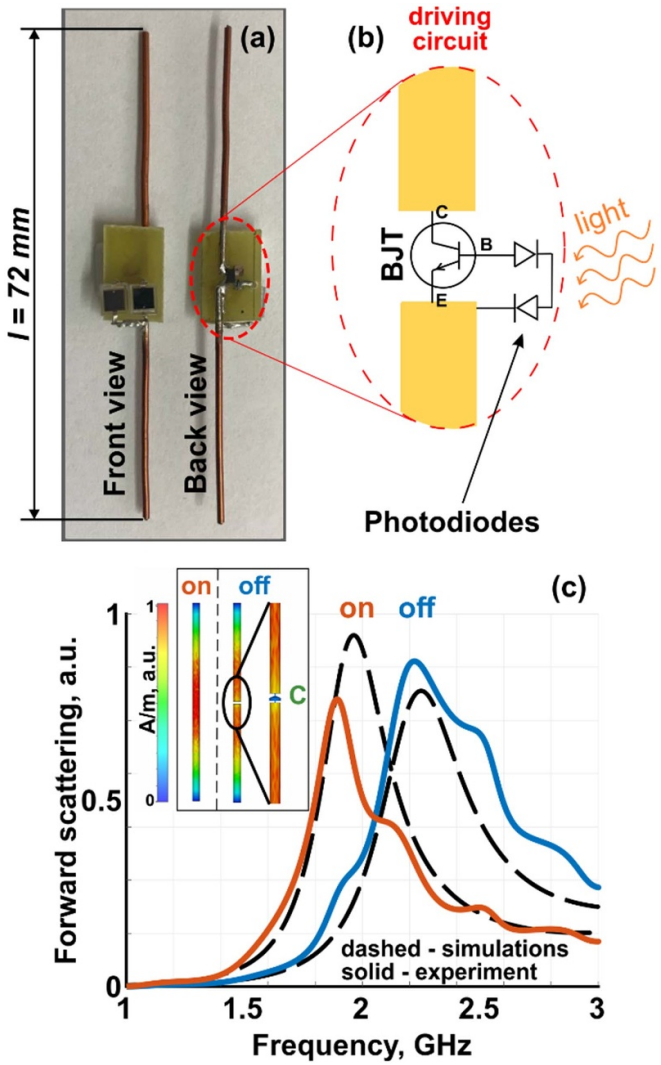

Figure 1. Optically-switchable passive element—photograph (a) and the schematics (b) of the photo-activated driving circuit (BJT—bipolar junction transistor, C—collector, B—base, and E—emitter). (c) Numerical analysis and experimental forward scattering spectra of the device at light 'on' and 'off' states. Color lines—responses of individual elements. Inset—current distributions along the elements (numerical results).

is 1 mm. Those parameters were tuned to make the device comply with IEEE 802.11 communication standards (in terms of radiation bands). It is worth mentioning that the transistor impedance is also considered for both open and short operation states. Figure 1(c) demonstrates the capability to tune the scattering peak from 2.2 GHz to 1.9 and vice versa upon light illumination. Full-wave numerical analysis, including an introduction of lumped elements, was done with CST Microwave Studio. The surface current distribution on the element strongly depends on the light state (insets to figure 1(c)), demonstrating the switching between dipolar and quadrupolar operation modes. 0.5 pF of the lumped element C was found to provide a reliable model for switching for the state 'off' and a solid $\lambda/2$ wire—for the state 'on'. Slight differences between numerical and experimental data come from nonvanishing form factors of active elements, which were not considered in simulations.

A choice of elements for implementing the driving circuit is worth a discussion. Among possible architectures (i) varactor + photodiode; (ii) PIN-photodiode and (iii) phototransistor or transistor + photodiode can be considered. While varactors are commonly used in related designs [16, 17], those are not the best candidates for the current implementation as they demand quite high voltage to provide a pF-scale capacitance tunability. 0.7 V for Si and 0.35 V for Ge implementations are required. Phototransistors are typically designed for low-frequency applications, e.g., fire protection or motion detection. Therefore, we will investigate a combination of a low-cost high-frequency BFU730F115 npn-type BJT and BPW34 photodiodes. The photodiode's anode is connected to the transistor's base and the cathode to the emitter (figure 1(b)). The collector and emitter of the transistor are the outputs of the driving circuit and are soldered to the $\lambda/4$ wires. This arrangement allows shifting the scattering resonance to higher frequencies.

3. Optically steerable antenna

After designing single elements, those will be assembled to form a larger-scale system, which aims to provide beam steering capabilities. Six passive director elements were chosen to form the geometry. This number, being found beneficial to optimize wire bundle scatterers [36–40], was chosen as a tradeoff between design simplicity and functionality. While this configuration fits the demands of a six-sector 4G wireless network, it can be further tuned per application, i.e. the number of scanning lobes can be increased, and various 5G communication protocols can be implemented.

The antenna consists of seven elements overall: one active (marked with '#') placed exactly at the center and six passives (1–6) are equidistantly distributed on an imaginary cylindrical surface (figure 2). A broadband monopole antenna (W1096), covering the investigated frequency range and providing rather flat frequency response, was chosen as a feed [41]. This commercial element can be replaced by a custom-made monopole, tuned per frequency. Before assembling the structure, each of the six passive elements was calibrated to provide an identical response (as in figure 1(c)). Here both scattering parameters and optical activation power are adjusted. Each individual element was checked separately by performing a forward scattering experiment. As the element acts as a dipole, this parameter almost completely characterizes its response. The manual adjustment was done by cutting the wire's length. It is also worth noting that nominals of lumped elements can vary from item to item. Hence, individual calibration is required. Figure 1(c) demonstrates the calibration curves, the average parameters of which were used in antenna modeling.

Without light activation, all six passive elements are identical and, as a result, the radiation pattern has no directivity in-plane (end-fire). To break the symmetry, several elements can be triggered with light. For an initial approximate analysis,

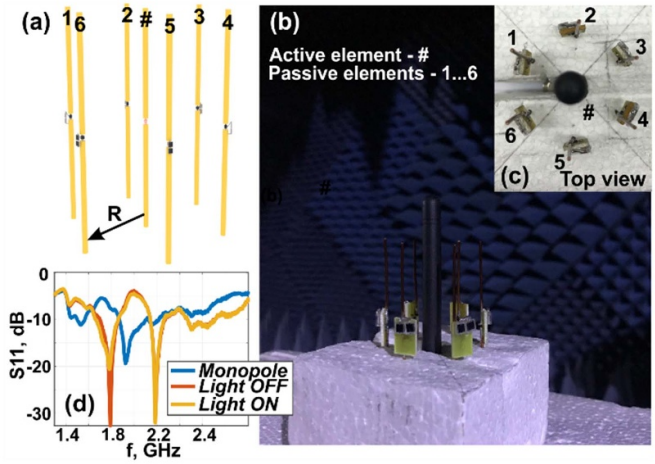

Figure 2. (a) Schematic layout and (b) photograph of the optically steerable antenna. On the insets (c) photograph of the top view. (d) S_{11} parameters of antennas—standalone monopole, steering antenna with light 'on and 'off', as in the legends.

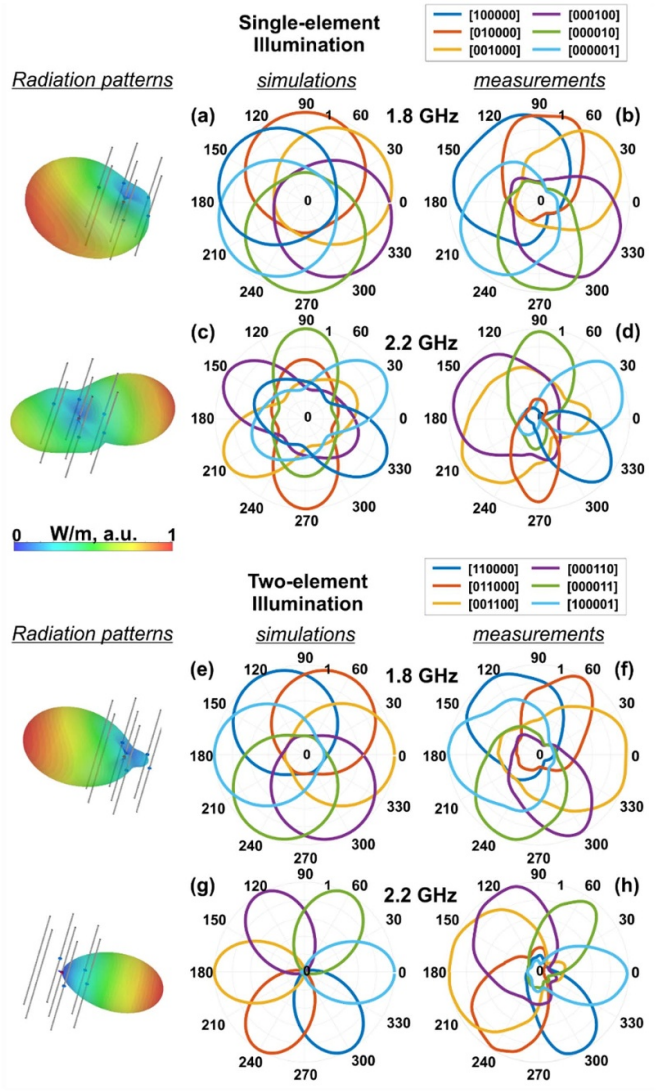

Figure 3. Radiation patterns—numerical and experimental results. Single (a)–(d) and double-element (e)–(h) illumination at the frequencies 1.8 (director case) and 2.2 GHz (reflector case). Antenna 3D radiation patterns (numerical results) are in left insets.

the elements can be considered as present for a 2.2 GHz wave if the light is 'on' and absent if there is no direct illumination on them. For 1.8 GHz the scenario is reversed. As a result, several elements form a directive pattern. A more accurate analysis suggests considering the impact of non-resonant inactivated elements. This was done numerically, and the system parameters were additionally optimized. The optimization is applied to maximize the directivity and gain of the antenna, constraining its overall size [42]. While directivity in a Yagi-Uda antenna relies on interference phenomena between several directors and reflectors, the proposed realization involves multipolar interaction and near-field coupling between elements [37–39]. The radius of the imaginary cylindrical surface (considering the cylinder radius $R = 20$ mm), containing optically switchable passive elements, was chosen to be 41 mm $\approx 0.26\lambda$. The 1.8 and 2.2 GHz were chosen quite arbitrarily within the wireless band and can be tuned per a specific application.

Figure 3 summarizes the patterns, obtained both numerically and experimentally at an anechoic chamber. '1' and '0' in the figure captions indicate whether the element was illuminated or not, respectively. Antenna matching conditions (S_{11} parameters) appear in figure 2(d). While the initial design was made for a single-element activation (figures 3(a)–(d)), different combinations can be considered as well. Theoretically, the system has $2N$ independent degrees of freedom, where N is the number of elements. Potentially, $2N$ antenna patterns can be achieved, nevertheless, not all of them can be considered practically relevant. Several reports have demonstrated N patterns with N tunable elements [32, 43, 44]. While our structure was not designed to maximize the number of patterns, we found that activating pairs of adjacent elements leads to the formation of directional beams, shifted by 30° with respect to the single-element case (figures 3(e)–(h)). As a result, we have demonstrated 12 directional beams, i.e. $2N$ useful patterns. Furthermore, the device shows a dual-band performance—both 1.8 and 2.2 GHz with a 10% fractional bandwidth. Activating other combinations of elements did not lead to the formation of patterns with reasonable directivity.

The directivity (D) and gain (G) of the antenna will be characterized next. As the pattern is formed primarily in-plane, the following relation will be used to process the experimental data [35]:

$$D(\varphi, \theta = \text{const}) = \frac{P_{\max}}{\frac{1}{2\pi}\int_0^{2\pi} P(\varphi)\,\mathrm{d}\varphi}, \tag{1}$$

where $P_{\max}$ is the maximal radiated power of the antenna. The assessment is made for a constant elevation angle ($\theta = 90°$, the z-axis is along the wires) and for the entire 2π of the azimuth φ. The realized gain G_{Tx} is extracted by comparing the device with an etalon antenna (IDPH-2018S/N-0807202 horn) with a known gain G_{Rx}. Equation (2) is used for the analysis [35]:

Table 1. The directivity D and differential gain G_{diff}.

			Numerical		Experimental
		f, GHz	2D	3D	2D
Single-element illumination	D, dBi	1.8	2.68	5.21	3.31
		2.2	2.48	5.17	4.11
	G_{diff}, dBi	1.8		2.06	2.65
		2.2		5.68	5.56
Two-element illumination	D, dBi	1.8	3.36	6.01	3.37
		2.2	6.17	9.27	3.85
	G_{diff}, dBi	1.8		2.49	2.2
		2.2		7.25	4.62

$$G_{Tx} = \left(\frac{4\pi a}{\lambda}\right)^2 \frac{P_{Rx}}{P_{Tx}} \frac{1}{G_{Rx}}, \tag{2}$$

where 'a' is the distance between the apertures of the transmit Tx and the receive Rx antennas, λ is the operational wavelength and $P_{Rx}/P_{Tx} = |S_{21}|^2$ is the power transmission coefficient.

To assess the switching parameter, we calculated the differential gain values between the 'on' and 'off' states (G_{on} and G_{off}), as follows:

$$G_{\text{diff}} = G_{\text{on}} - G_{\text{off}}. \tag{3}$$

The results are summarized in table 1. The numerical results on directivity are presented for the 2D ($\varphi,\theta = 90°$) and 3D (φ,θ) cases, while the experiments are shown only for the 2D case. One can see the difference between the directivity of numerical and experimental values, especially at 2.2 GHz. The results can be assessed by comparing patterns in figure 3. The most pronounced difference was found for the data on panels (c) and (d). A significant back lobe, being predicted numerically (imperfect optimization), was not found in the measurements. The opposite behavior was found for the two-element illumination at 2.2 GHz—here back lobes were found in the experiment, while the numerical prediction suggests rather minor back radiation. The reason for this can be several-fold: (i) imperfection in elements, affecting the interference phenomena, and (ii) a parasitic illumination due to the ambient illumination and the pollution from nearby light sources—the driving LED (as will be discussed hereinafter). Nevertheless, the back lobe suppression effect is not dramatic. (iii) Nevertheless, the feeding monopole connector has an orientation, perpendicular to the antenna axis, it breaks the symmetry between different radiation patterns (e.g. yellow, and purple lines in figure 3). Also, note, that the differential gain can be larger than the directivity, as it considers the difference between two states of the system.

It is worth mentioning that the system cannot perform an independent simultaneous beam steering at two different frequency bands, as the same photodiodes are in use.

Free-space illumination of photodiodes requires extra consideration. The first factor is ambient radiation, which can accidentally bring the system to a threshold. For an assessment, we compared chamber conditions with an office space and outdoors (direct summer sunlight). In the last two cases, a light concealment arrangement is required to maintain the correct operation of the device. The second factor is undesired light from a nearby illuminated element. The distance between the LED and the photodiode is 1 cm (inset to figure 4(a)), thus the light leakage was found to play no role—table 2 summarizes the claim. In both cases, the voltage on the diode was measured and compared with the 0.7 V threshold. It is worth noting that introducing integrated optics arrangements (e.g. waveguiding devices or lasers) can solve issues of undesired overexposure to light.

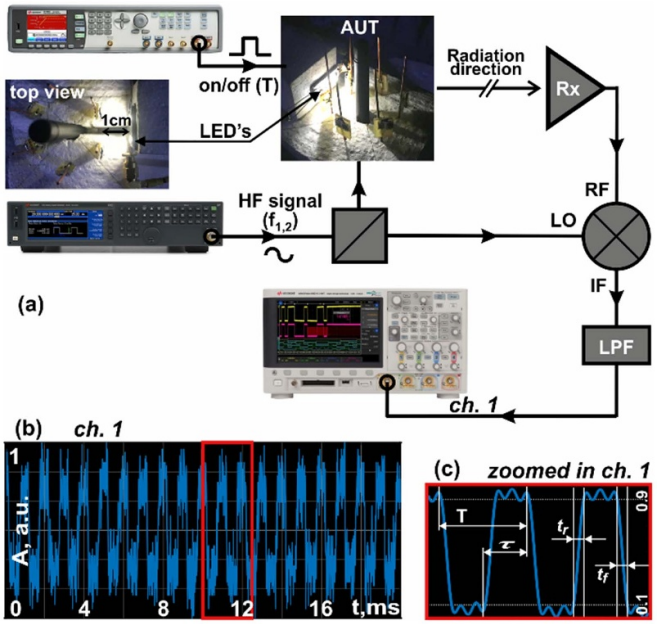

Figure 4. (a) Schematics of the setup for measuring the switching rate. (b) Zoomed IF signal on the scope. (c) Post-processed signal—period $T = 1$ ms (50% duty cycle for $\tau = 0.5$ ms), rise t_{r}, and fall t_{f} time.

One of the main advantages of the proposed design is its potentially fast switching rates. The 5G standards demand latencies as small as a millisecond. It implies having capabilities of kHz beam steering rates. To assess this parameter, the following setup has been constructed—a signal from a

Table 2. Voltage drop on illuminated diodes.

Distance (cm)	Voltage on illuminated diode (V)	Voltage on adjusting diode (V)
1	0.82	0.58
1.5	0.8	0.59
2	0.775	0.59
2.5	0.72	0.58
3	0.7	0.575
3.5	0.68	0.57
4	0.66	0.56

high-frequency generator (N5173B EXG X-Series Microwave Analog Signal Generator) is split via ZX10-2-852-S+ Splitter into two channels: the first feeds the active element of the antenna and the second provides the synchronization signal and feeds the local oscillator (LO) input of a mixer ZX05-C24-S+ at the receiver (figure 4(a)). The LF pulse sequences generator (81 160 A Pulse Function Arbitrary Noise Generator) feeds a LED SMD5630, which is located close to the antenna photodiodes and performs the on/off-switching with a period $T = 1$ ms. 50% duty cycle (τ) was chosen. The receiver includes an Rx antenna, feeding the RF input of the mixer. The output, after a low-pass filter BLP-100-75+, is displaced on a scope. The digitalized scope's output allows investigation switching properties of the device (antenna under test—AUT). The results show that $f_0 = 1/T$ at 1 kHz can be obtained (figure 4(b)). To determine rise (t_r) and fall (t_f) times, the received signal was smoothed and fitted with a sine series (figure 4(c)). The extracted rise and fall times for the system are ∼0.1 ms.

4. Beam steering with other antennas

To demonstrate the flexibility of the proposed method, three different antennas have been considered, namely the commercial monopole from the previous studies, a symmetric dipole antenna, and a monopole above a ground plane (panels (a), (c), and (e) in figure 5, respectively). Each of those has an omnidirectional pattern in-plane. Two switching elements have been used to demonstrate the concept. As the structures have reflection symmetry, only one directional pattern per frequency was demonstrated. Yellow and green lines correspond to 2.2 and 1.8 GHz, respectively. Illuminating one side of the structure leads to the creation of directional patterns, which are oppositely oriented for both of those frequencies. Switching between the illumination sides will cause a flip in the patterns. The commercial monopole antenna has slightly better performance. The dipole demonstrates a less directive pattern at 1.8 GHz owing to the frequency-dependent balun. This aspect does not affect the monopole configuration, which also demonstrates good switching capabilities. It is also worth briefly noting that the operational bandwidth of the demonstrated elements is ∼200 MHz, which is 10% of the carrier frequency, complying with the wireless communication needs.

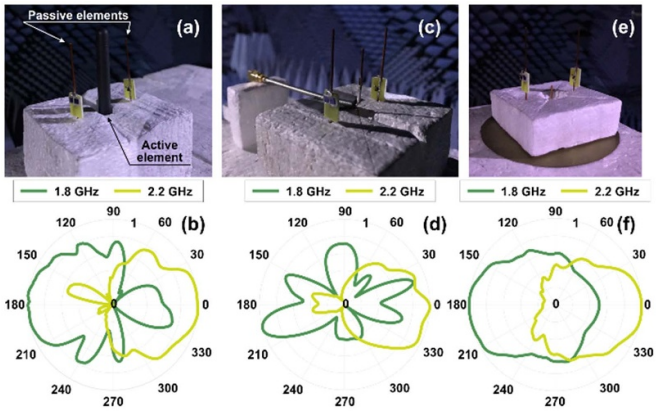

Figure 5. The concept of granting a radiating element with beam steering capabilities. (a), (c), and (e)—Photographs of antenna devices. (b), (d), and (f)—Experimentally obtained (in-plane) radiation patterns. Switching between 2 sectors has been considered.

5. Conclusion

A scanning antenna with optical control is demonstrated experimentally. The device consists of six passive resonators, arranged around the feed. Electromagnetic properties of passive elements, serving as either directors or reflectors, are tuned with light. The driving circuit, containing photodiodes and a bipolar transistor, is activated remotely with light. This approach allows tuning electromagnetic properties of the system without a need for a branched network of metal wires. The demonstrated design provides steering capabilities of directional beams with ∼5–6 dBi (3D simulations) and ∼3–4 dBi (2D experiment) of the directivity and ∼2–7 dBi (3D simulations) and ∼2–5 dBi (2D experiment) of the differential gain with a switching rate around at kHz rate. The demonstrated antenna belongs to the class of compact ($2\ r/\lambda \approx 0.5$–0.6, where r is the radius of an imaginary sphere that surrounds the whole antenna [42, 45]) low-cost devices (the active element + six passive elements with driving circuits as well as LED and pulse signal circuit cost around 22$). Furthermore, it was shown to provide dual-band operation at frequencies, relevant to wireless communications. Further optimization of the electromagnetic design and introduction of fast elements (transistors and fast photodiodes) can elevate the switching rates towards MHz and higher opening pathways to new applications, where fast beam steering and beamforming performances are required (e.g. radars and 5G). Frequency bands in 5G protocols are quite broad and utilized per application, though the capability of fast beam control remains essential. It is worth noting that a volumetric arrangement of switchable elements can allow for scanning in elevation on pathways for obtaining capabilities of scanning the entire 4π sphere. Considering radar applications, where degree level and lower angular resolutions are required, will demand using a larger number of elements (e.g. arrays, encompassing 10 s and hundreds of elements). In this case, reducing the number of control wires, and replacing them with an optical link, can be beneficial.

The light activation approach allows constructing devices with multiple almost non-interacting degrees of freedom, as a branched feeding network is not required and, in principle, almost any radiating element can be granted with beam steering capabilities. This approach is rather generic and can be replicated to NIR, THz, or any spectral range, constrained by technological availability.

Data availability statement

All data that support the findings of this study are included within the article (and any supplementary files).

Acknowledgments

The work was supported by ERC POC, Grant 101061890 'DeepSight'. T S was funded by the Latvian Council of Science project: Novel complex approach to the optical manipulation of Nanoparticles (PHOTON), No. lzp-2022/1-057, and by Latvian Quantum Technologies Initiative (2.3.1.1.i.0/1/22/I/CFLA/001).

Conflict of interest

The authors declare that they have no known competing financial interests or personal relationships that could have appeared to influence the work reported in this paper.

ORCID iD

Dmytro Vovchuk https://orcid.org/0000-0001-7108-8984

References

[1] Patole S M, Torlak M, Wang D and Ali M 2017 Automotive radars: a review of signal processing techniques *IEEE Signal Process. Mag.* **34** 22–35
[2] Asensio-López A, Blanco-del-campo A, Gismero-Menoyo J, Ramirez-Morán D, Torregrosa-Penalva G, Pablo Dorta-Naranjo B and Carmona-Duarte C 2004 High range-resolution radar scheme for imaging with tunable distance limits *Electron. Lett.* **40** 1085–6
[3] MathWorks 2017 5G development with MATLAB *MathWorks*
[4] Gimmestad G G and Roberts D W *Lidar Engineering : Introduction to Basic Principles* (Cambridge University Press) p 341
[5] LiDAR Remote Sensing and Applications Pinliang Dong, Qi Chen—Google книги (available at: https://books.google.co.il/books?hl=uk&lr=&id=jXFQDwAAQBAJ&oi=fnd&pg=PP1&dq=lidar+book&ots=j9UUq94hPy&sig=iy3LBLZlOTKwRacTzPii9M2VUUw&redir_esc=y#v=onepage&q=lidar%20book&f=false) (Accessed 9 July 2023)
[6] Intel Corporation Intel 5G Standards and Spectrum (available at: www.intel.com/content/www/us/en/wireless-network/5g-technology/standards-and-spectrum.html) (Accessed 21 June 2022)
[7] Ford R, Zhang M, Mezzavilla M, Dutta S, Rangan S and Zorzi M 2017 Achieving ultra-low latency in 5G millimeter wave cellular networks *IEEE Commun. Mag.* **55** 196–203
[8] Patan Saleem A 2021 Beam steering in microstrip patch antenna by using psebg (available at: www.google.co.il/books/edition/BEAM_STEERING_IN_MICROSTRIP_PATCH_ANTENN/nVVHEAAAQBAJ?hl=uk&gbpv=0) (Accessed 9 July 2023)
[9] RadarBox DIGITAL LINE (available at: https://diedrichs-schiffstechnik.de/downloads/)
[10] Horstmann J, Bödewadt J, Carrasco R, Cysewski M, Seemann J and Streβer M 2021 A coherent on receive X-band marine radar for ocean observations *Sensors* **21** 7828
[11] Stimson G W 1998 *Introduction to Airborne Radar* (SciTech Pub.) (https://doi.org/10.1049/SBRA101E)
[12] Engheta N and Ziolkowski R 2006 *Electromagnetic Metamaterials: Physics and Engineering Explorations* (Wiley)
[13] Filonov D, Shmidt A, Boag A and Ginzburg P 2018 Artificial localized magnon resonances in subwavelength meta-particles *Appl. Phys. Lett.* **113** 123505
[14] Asadchy V S, Albooyeh M, Tcvetkova S N, Díaz-Rubio A, Ra'Di Y and Tretyakov S A 2016 Perfect control of reflection and refraction using spatially dispersive metasurfaces *Phys. Rev.* B **94** 075142
[15] Capolino F 2017 *Applications of Metamaterials* (Taylor & Francis) (https://doi.org/10.1201/9781420054248/APPLICATIONS-METAMATERIALS-FILIPPO-CAPOLINO)
[16] Zheludev N I and Kivshar Y S 2012 From metamaterials to metadevices *Nat. Mater.* **11** 917–24
[17] Kozlov V, Vovchuk D and Ginzburg P 2021 Broadband radar invisibility with time-dependent metasurfaces *Sci. Rep.* **11** 1–11
[18] Faenzi M, Minatti G, González-Ovejero D, Caminita F, Martini E, Della Giovampaola C and Maci S 2019 Metasurface antennas: new models, applications and realizations *Sci. Rep.* **9** 1–14
[19] Quevedo-Teruel O *et al* 2019 Roadmap on metasurfaces *J. Opt.* **21** 073002
[20] Wang J, Li Y, Jiang Z H, Shi T, Tang M-C, Zhou Z, Chen Z N and Qiu C-W 2020 Metantenna: when metasurface meets antenna again *IEEE Trans. Antennas Propag.* **68** 1332–47
[21] Markovich H, Filonov D, Shishkin I and Ginzburg P 2018 Bifocal Fresnel lens based on the polarization-sensitive metasurface *IEEE Trans. Antennas Propag.* **66** 2650–4
[22] Kozlov V, Filonov D, Shalin A S, Steinberg B Z and Ginzburg P 2016 Asymmetric backscattering from the hybrid magneto-electric meta particle *Appl. Phys. Lett.* **109** 203503
[23] Filonov D, Kozlov V, Shmidt A, Steinberg B Z and Ginzburg P 2018 Resonant metasurface with tunable asymmetric reflection *Appl. Phys. Lett.* **113** 094103
[24] Xu H-X, Tang S, Ma S, Luo W, Cai T, Sun S, He Q and Zhou L 2016 Tunable microwave metasurfaces for high-performance operations: dispersion compensation and dynamical switch *Sci. Rep.* **6** 38255
[25] Sievenpiper D F, Schaffner J H, Song H J, Loo R Y and Tangonan G 2003 Two-dimensional beam steering using an electrically tunable impedance surface *IEEE Trans. Antennas Propag.* **51** 2713–22
[26] Yang W, Gu L, Che W, Meng Q, Xue Q and Wan C 2019 A novel steerable dual-beam metasurface antenna based on controllable feeding mechanism *IEEE Trans. Antennas Propag.* **67** 784–93
[27] Wang X and Tretyakov S 2021 From tunable and reconfigurable to space-time modulated multifunctional

metasurfaces *2021 IEEE Int. Symp. on Antennas and Propagation and North American Radio Science Meeting, APS/URSI 2021—Proc.* pp 1361–2
[28] Di Renzo M, Zappone A, Debbah M, Alouini M-S, Yuen C, de Rosny J and Tretyakov S 2020 Smart radio environments empowered by reconfigurable intelligent surfaces: how it works, state of research, and the road ahead *IEEE J. Sel. Areas Commun.* **38** 2450–525
[29] Ramaccia D, Sounas D L, Alu A, Toscano A and Bilotti F 2020 Phase-induced frequency conversion and Doppler effect with time-modulated metasurfaces *IEEE Trans. Antennas Propag.* **68** 1607–17
[30] Luther J J, Ebadi S and Gong X 2012 A microstrip patch electronically steerable parasitic array radiator (ESPAR) antenna with reactance-tuned coupling and maintained resonance *IEEE Trans. Antennas Propag.* **60** 1803–13
[31] Sun C, Hirata A, Ohira T and Karmakar N C 2004 Fast beamforming of electronically steerable parasitic array radiator antennas: theory and experiment *IEEE Trans. Antennas Propag.* **52** 1819–32
[32] Rzymowski M, Duraj D, Kulas L, Nyka K and Woznica P 2016 UHF ESPAR antenna for simple angle of arrival estimation in UHF RFID applications *2016 21st Int. Conf. on Microwave, Radar and Wireless Communications, MIKON 2016* (https://doi.org/10.1109/MIKON.2016.7491984)
[33] Dobrykh D, Mikhailovskaya A, Ginzburg P and Filonov D 2020 4D optically reconfigurable volumetric metamaterials *Phys. Status Solidi* **14** 2000159
[34] 2020 Antenna array and a system employing the same USA Pathent, US20210083377A1 (available at: https://patents.google.com/patent/US20210083377A1/en)
[35] Balanis C A 2005 *Antenna Theory: Analysis and Design* 3rd edn (Wiley)
[36] King R W P, Fikioris G J and Mack R B 2002 *Cylindrical Antennas and Arrays* (Cambridge University Press)
[37] Vovchuk D, Kosulnikov S, Noskov R E and Ginzburg P 2020 Wire resonator as a broadband Huygens superscatterer *Phys. Rev.* B **102** 094304
[38] Kosulnikov S, Vovchuk D, Noskov R E, Machnev A, Kozlov V, Grotov K, Ladutenko K, Belov P and Ginzburg P 2022 Circular wire-bundle superscatterer *J. Quant. Spectrosc. Radiat. Transfer.* **279** 108065
[39] Grotov K *et al* 2022 Genetically designed wire bundle super-scatterers *IEEE Trans. Antennas Propag.* **70** 1
[40] Kosulnikov S Y, Mirmoosa M S, Vovchuk D A, Tretyakov S A, Glybovski S B and Simovski C R 2016 Enhancement of radiation with irregular wire media *IEEE Trans. Antennas Propag.* **64** 5469–74
[41] Pulse A Technitrol Company W1095X datasheet (PDF)—pulse A Technitrol Company (available at: www.alldatasheet.com/datasheet-pdf/pdf/1320661/PULSE/W1095X.html) (Accessed 21 June 2022)
[42] Pigeon M, Delaveaud C, Rudant L and Belmkaddem K 2014 Miniature directive antennas *Int. J. Microw. Wirel. Technol.* **6** 45–50
[43] Lee K P and Choi H K 2016 Five-element ESPAR antenna using the annular ring slot active element *Microw. Opt. Technol. Lett.* **58** 2800–4
[44] Liang Q, Sun B and Zhou G 2018 Multiple beam parasitic array radiator antenna for 2.4 GHz WLAN applications *IEEE Antennas Wirel. Propag. Lett.* **17** 2513–6
[45] Geyi W 2003 Physical limitations of antenna *IEEE Trans. Antennas Propag.* **51** 2116–23